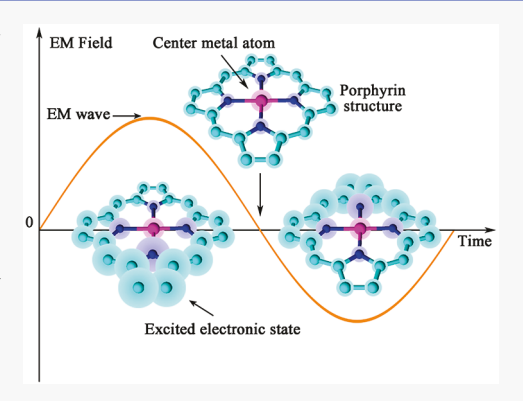


# Photonically-Activated Molecular Excitations for Thermal Energy **Conversion in Porphyrinic Compounds**

Yuan Zhao, † Jou Lin, † David M. Kundrat, † Mathias Bonmarin, ‡ John Krupczak Jr., § Som V. Thomas, † Mengyao Lyu, † and Donglu Shi\*, †

ABSTRACT: Heterocyclic, macrocycle organic compounds, structurally characterized with porphyrins, are not only abundant in nature but also environmentally friendly. These porphyrinic compounds have recently been extensively studied for their fascinating structures, physical properties, and high potentials in engineering applications. We report experimental results on the photonically activated thermal energy conversion via irradiations of white light (simulated solar light). The photothermal effects have been well studied for metallic conductors with a large number of charge carriers based on the socalled localized surface plasmon resonance (LSPR). However, the LSPR model may not apply to the porphyrinic materials with a very limited number of charge carriers. In this study, we have found several porphyrinic compounds to exhibit pronounced photothermal effects including chlorophyll, chlorophyllin, hemoglobin, and phthalocyanine, which all share similar structural characteristics. Raman data show characteristic molecular vibrations from



these compounds that are responsible for photon-to-thermal energy conversions near the optical absorption frequencies. We attribute the porphyrin molecular vibrations to the photothermal effects observed from these compounds and predict that all porphyrinic materials can be optically activated for pronounced photothermal effects. Also established is a newly defined specific photothermal coefficient (SPC), a unique photothermal property of the thin films investigated in this study.

#### 1. INTRODUCTION

A group of heterocyclic macrocycle organic compounds shares a common structural feature, namely, porphyrin, composed of four modified subunits bounded with carbon atoms forming a "ringlike" structure, therefore also known as "porphyrin rings" (Figure 1). There are 26  $\pi$ -electrons in each porphyrin structure, and 18 of them form a continuous cycle of conjugated bonds, as illustrated in Figure 1. These unique macrocycle organic compounds have been extensively studied in terms of structural characteristics, bonding mechanisms, electronic and molecular behaviors, <sup>4-7</sup> conductivity, <sup>8-10</sup> and structural-related physical properties. <sup>11,12</sup> Although the majority of the previous work focuses on the fundamental porphyrin science, significant attention has been increasingly drawn to the potential engineering applications, especially in the recent years. 13,14 In all previous work, many studies focused on the conductivity 15-17 and ferroelectricity 11,12 underlying the electronic structures of porphyrins.

A fascinating feature of porphyrins that has only been recently discovered is that the group of heterocyclic macrocycle organic compounds with porphyrins is capable of converting photons to thermal energy quite efficiently. 14 As it is well-known, all these compounds exhibit unique, distinctive, and intrinsic photon absorption spectra in a wide range of frequencies from UV to NIR. Each spectrum is specifically associated with the metal ion that is bonded to all four nitrogen atoms. For instance, for chlorophyll with a magnesium center atom, the typical absorption is characterized by a saddlelike shape with two peaks at 420 and 660 nm, respectively, therefore appearing 'green" (Figure 1a). A similar absorption spectrum is shown in Figure 1b for chlorophyllin. For hemoglobin, the center metal atom in porphyrin is iron and its absorption spectrum exhibits one sharp peak at 400 nm, resulting in a red color (Figure 1c). Phthalocyanine is closely related to porphyrin. Copper phthalocyanine exhibits a blue color with a distinctive spectrum (Figure 1d). In this fashion, i.e., via replacement of center atoms, various porphyrins can be formed with more than 50 metals and semimetals. Upon light irradiation, all porphyrinic compounds absorb light variably at different frequencies and consequently generate thermal energy that can be typically observed via the temperature versus time heating curves, known as the photothermal effect. Recently, some porphyrinic compounds have been reported for their pronounced photothermal effects, including heme, chlorophyll, and zinc porphyrin. 14,18-20

Received: October 4, 2019 Revised: November 19, 2019 Published: December 18, 2019

1575

<sup>&</sup>lt;sup>†</sup>The Materials Science and Engineering Program, Department of Mechanical and Materials Engineering, College of Engineering and Applied Science, University of Cincinnati, Cincinnati, Ohio 45221, United States

<sup>&</sup>lt;sup>‡</sup>School of Engineering, Zurich University of Applied Sciences, Winterthur 8400, Switzerland

Department of Engineering, Hope College, Holland, Michigan 49423, United States

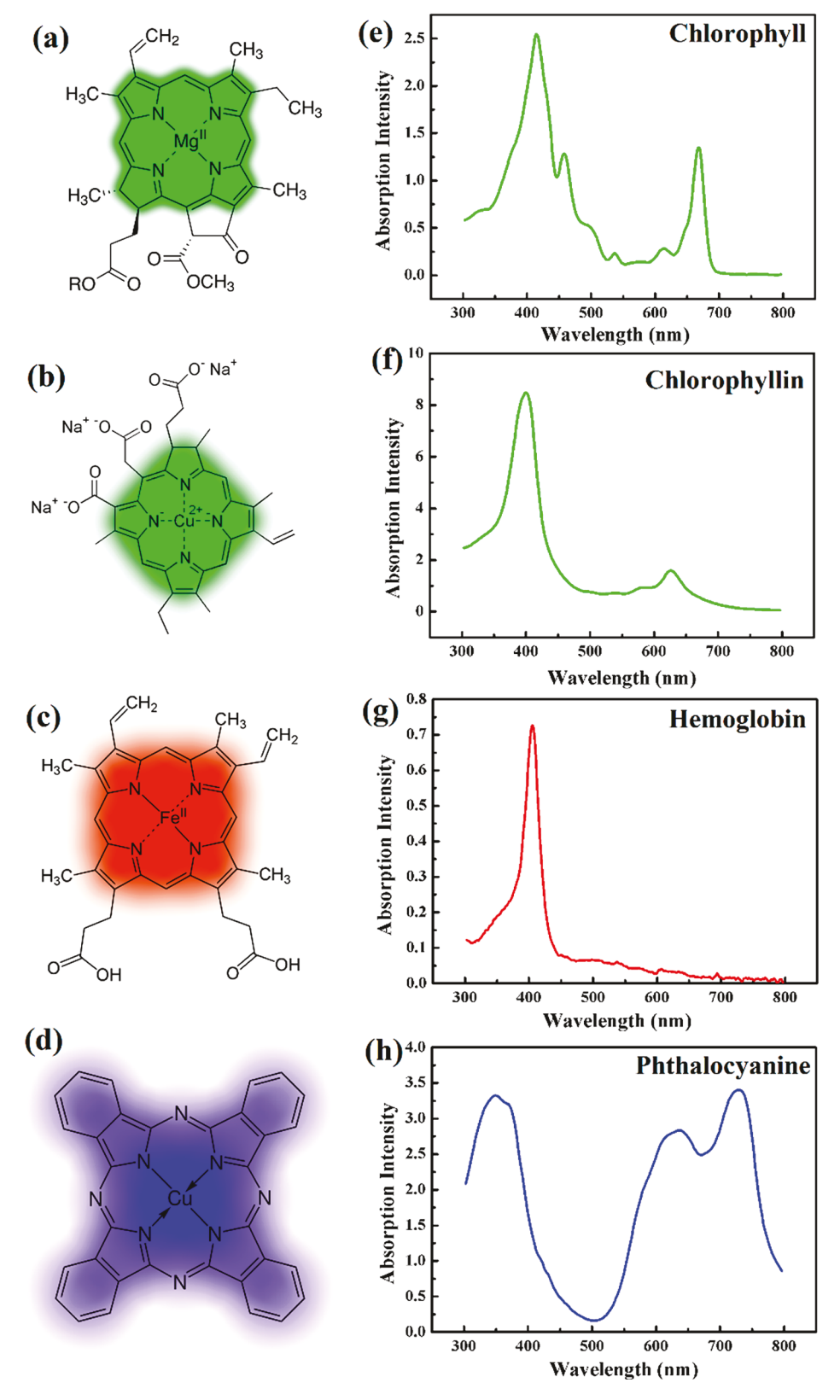


**Figure 1.** Schematic diagrams of various porphyrin structures: (a) chlorophyll a, (b) chlorophyllin sodium copper, (c) heme-b, and (d) copper phthalocyanine and corresponding absorption spectra of (e) chlorophyll extract (Chl), (f) chlorophyllin sodium copper (Chlin), (g) hemoglobin (HB), and (h) copper phthalocyanine (Phth). All absorption spectra are obtained in solution forms of the same concentration (0.01 mg/mL): Chl in toluene, Chlin in water, HB in PBS, and Phth in DMSO.

The photothermal effect is associated with the electronic or molecular interactions with electromagnetic radiation, be it monochromatic or white light. The photonically activated electronic and molecular excitations can result in the production of thermal energy (heat). The photothermal effect has been well studied for metallic conducting materials, most extensively on

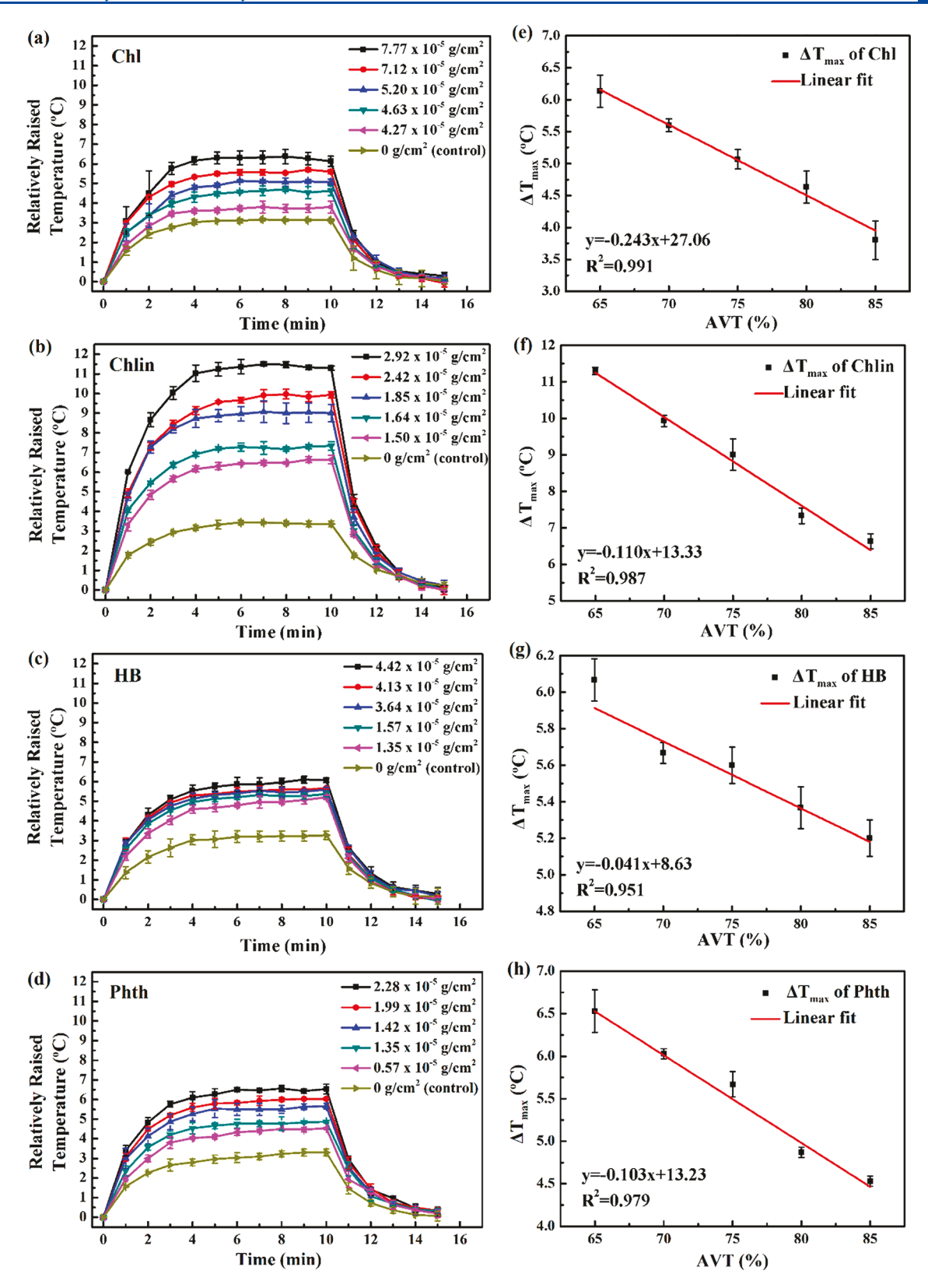


Figure 2. Temperature difference  $\Delta T$  vs time for (a) Chl samples, (b) Chlin, (c) HB, and (d) Phth, with concentrations indicated.  $\Delta T_{\text{max}}$  vs AVT for (e) Chl samples, (f) Chlin, (g) HB, and (h) Phth. All samples are irradiated by simulated solar light (0.1 W/cm<sup>2</sup>).

gold,<sup>21</sup> silver,<sup>22</sup> and graphene,<sup>23</sup> which are typically characterized with high densities of charge carriers.<sup>21,22,24</sup> The photothermal effect mechanism has been identified as the so-called localized surface plasmon resonance (LSPR).<sup>21,24,25</sup>

LSPR results from the confinement of a surface plasmon in a nanoparticle smaller than the wavelength of the incident light. A nanoparticle's response to the oscillating electric field can be described by the so-called dipole approximation of Mie theory.<sup>26</sup>

Table 1. Parameters of the Chl Films under White Light Irradiation (0.1 W/cm<sup>2</sup>)<sup>a</sup>

	AVT, %	$ ho_{ m pm}$ , g/cm <sup>2</sup>	$\Delta T_{ m max}$ $^{\circ}$ C	$U, W/(m^2 \cdot K)$	Q, J/s	efficiencyη, %
Chl-S-1	64.7	$7.77 \times 10^{-5}$	6.13	15.68	0.135	20.9
Chl-S-2	69.8	$7.13 \times 10^{-5}$	5.60	16.86	0.132	20.5
Chl-S-3	75.3	$5.21 \times 10^{-5}$	5.07	13.54	0.096	14.9
Chl-S-4	79.8	$4.64 \times 10^{-5}$	4.63	15.63	0.102	15.7
Chl-S-5	84.3	$4.28 \times 10^{-5}$	3.80	13.84	0.074	11.4

<sup>&</sup>quot;The photothermal material density on the glass,  $\rho_{\rm pm}$ , represents the mass of thin film per coating area (g/cm²),  $\Delta T_{\rm max}$  is the maximum steady temperature difference, U is the heat transfer coefficient (W/(m²·K)),  $\dot{Q}$  is the heat produced via photothermal effect in unit of time (J/s), and  $\eta$  is the photothermal efficiency.

At the plasmonic resonance, the electric fields near the particle surface are greatly enhanced. This enhancement falls off quickly with distance from the surface. The optical absorption of the particle is therefore approaching a maximum at the plasmon resonant frequency. For noble metal nanoparticles, this occurs at visible wavelengths. The dissipation of LSPR in the form of thermal energy gives rise to a temperature increase.

Noble metals and porphyrinic compounds are sharply juxtaposed with conductivity; while the former is  $4.5 \times 10^7$  S/ m, the latter is on the order of 10<sup>-7</sup> S/m for a tetragonal porphyrin single crystal. 15,16 Low-energy gaps have been reported for various porphyrin compounds on the order of a few electronvolts, with an absorption up to 900 nm.<sup>27</sup> However, the photothermal mechanisms of porphyrinic compounds have, to our knowledge, never been identified, especially in correlation with photon-porphyrin interactions. In contrast to noble metals, porphyrins contain a large number of conjugated bonds but lack charge carriers. Therefore, the operating mechanisms must be fundamentally different between these two classes of materials. In this study, we report the photothermal effects observed from four typical porphyrinic compounds, namely, chlorophyll, chlorophyllin, hemoglobin, and phthalocyanine, and identify the possible mechanisms of photonically activated molecular excitations. Also reported is a newly defined parameter: a specific photothermal coefficient (SPC) that is established on the basis of the photothermal data from the thin film samples.

## 2. METHODS

Chlorophyll (Chl) was extracted from spinach on the basis of a method previously reported.<sup>14</sup> Specifically, fresh local spinach leaves were cut into small pieces ( $\sim$ 5 × 5 mm<sup>2</sup>) and then freezedried at -40 °C for 48 h. The dry leaves (5 g) were washed twice using petroleum ether (boiling point 40-60 °C) to remove the carotenoids and waxes. The washed leaves were immersed and stirred in 300 mL of methanol/petroleum ether (3:1 v/v) at room temperature overnight. The remaining solids were removed by filtration, and the solution was transferred to a separatory funnel and then washed twice with 200 mL of saturated sodium chloride solution. The organic phase was filtrated and removed by rotary evaporation. The isolated film was then dissolved in 50 mL of acetone and stored at -20 °C for 24 h to precipitate impurities. Precipitates were pelleted by centrifugation, and the supernatant was collected. Acetone was removed by rotary evaporation. The isolated chlorophyll was dissolved in toluene, and the solution was stored at -20 °C until use. Chlorophyllin sodium copper was purchased from Sigma-Aldrich, hemoglobin (source: Bovine Erythrocytes) was purchased from Worthington Biochemical Corporation, and copper phthalocyanine ( $\beta$ -form) was purchased from Tokyo Chemical Industry Co., Ltd.

For the thin film deposition, the Chl solution was mixed with PMMA in toluene, while Chlin was mixed with PEG in water. The phthalocyanine (copper(II) phthalocyanine) and hemoglobin (HB) powders (both mixed with PEG) were dissolved in DMSO and PBS buffer, respectively, to form solutions. The concentrations of PMMA and PEG were maintained at 5 wt % for each solution. All solutions were applied uniformly on the glass substrates by spin coating 120  $\mu$ L of solutions at 1000 rpm for 30 s on glass slides (via WS-400-6NPP-Lite spin coater). The glass slides were pretreated by cutting into 25 × 25 mm<sup>2</sup> substrates and cleaned by sonication in methanol for 15 min, followed by sonication in isopropyl alcohol for another 15 min. The thickness of the coated samples on glass substrates was varied to investigate the average visible transmittance (AVT) in the range 380-760 nm, a key factor in the photothermal effect. AVT values were measured by using an LS116 light transmittance meter (manufactured by Linshang Technology).

Temperature vs time curves were obtained for all samples irradiated at different power densities. A solar simulator with controllable power supply was set upon samples for light irradiation (0.1  $\rm W/cm^2$ ). The shape and size of the light spot were set to exactly cover the sample well. The sample temperature was recorded by an FLIR camera aimed at the central surface of the sample. The surface sample emissivity was set to 0.92 for all samples.

### 3. RESULTS

Figure 2 shows photothermal experimental results of chlorophyll (Chl), chlorophyllin (Chlin), hemoglobin (HB), and phthalocyanine (Phth) thin films on glass substrates irradiated by the simulated solar light. A Newport 150 W solar simulator was employed with an intensity of 0.1 W/cm² for generating the photothermal effect. Parts a–d of Figure 2 show the temperature raised from the background room temperature ( $\Delta T$ ) by light irradiation, as a function of time for the Chl (Figure 2a), Chlin (Figure 2b), HB (Figure 2c), and Phth (Figure 2d) samples, with different concentrations indicated. These specific concentrations result in different AVT values (65%, 70%, 75%, 80%, 85%, and control sample, respectively).

As can be seen in this figure, the temperatures increase quite rapidly in the first 2–3 min for all films of different concentrations but slow down and form plateaus after 5 min. There are two competing factors that dominate the heating curves, the photonically generated heat responsible for the temperature rise and the heat loss through the thin film surface and the substrate. At the beginning, the heating is greater than the heat loss, therefore leading to a rather rapid temperature increase. However, heating is subsequently balanced by the heat loss, developing a plateau that can extend for a prolonged period of time, as long as the light source is provided. As can also be seen in this figure, the light is turned off at 10 min, resulting in an

Table 2. Parameters of the Chlin Films under White Light Irradiation (0.1 W/cm<sup>2</sup>)

	AVT, %	$ ho_{ m pm}$ , g/cm $^2$	$\Delta T_{ m max}$ $^{\circ}{ m C}$	$U, W/(m^2 \cdot K)$	Ċ, J∕s	efficiency $\eta$ , %
Chlin-S-1	64.5	$2.92 \times 10^{-5}$	11.30	15.02	0.238	36.9
Chlin-S-2	70.8	$2.42 \times 10^{-5}$	9.93	14.54	0.203	31.4
Chlin-S-3	74.7	$1.85 \times 10^{-5}$	9.00	14.54	0.183	28.4
Chlin-S-4	80.1	$1.64 \times 10^{-5}$	7.33	14.65	0.151	23.4
Chlin-S-5	85.2	$1.49 \times 10^{-5}$	6.63	14.43	0.134	20.8

Table 3. Parameters of the HB Films under White Light Irradiation (0.1 W/cm<sup>2</sup>)

	AVT, %	$ ho_{ m pm}$ , g/cm $^2$	$\Delta T_{ m max}$ $^{\circ}$ C	$U, W/(m^2 \cdot K)$	Q, (J/s)	efficiency $\eta$ , %
HB-S-1	64.8	$4.42 \times 10^{-5}$	6.07	12.23	0.104	16.1
HB-S-2	69.7	$4.13 \times 10^{-5}$	5.67	14.03	0.111	17.3
HB-S-3	75.4	$3.64 \times 10^{-5}$	5.60	12.07	0.095	14.7
HB-S-4	80.4	$1.57 \times 10^{-5}$	5.37	13.51	0.102	15.8
HB-S-5	84.5	$1.36 \times 10^{-5}$	5.20	14.16	0.103	16.0

Table 4. Parameters of the Phth Films under White Light Irradiation (0.1 W/cm<sup>2</sup>)

	AVT, %	$ ho_{ m pm}$ , ${ m g/cm}^2$	$\Delta T_{ m max}$ $^{\circ}{ m C}$	$U, W/(m^2 \cdot K)$	Q (J/s)	efficiency $\eta$ , %
Phth-S-1	64.5	$2.28 \times 10^{-5}$	6.53	11.67	0.107	16.6
Phth-S-2	69.7	$2.00 \times 10^{-5}$	6.03	11.37	0.096	14.9
Phth-S-3	75.1	$1.42 \times 10^{-5}$	5.67	12.00	0.095	14.8
Phth-S-4	80.5	$1.35 \times 10^{-5}$	4.87	10.91	0.075	11.6
Phth-S-5	85.5	$5.69 \times 10^{-5}$	4.53	11.02	0.070	10.9

exponential decrease of temperature for all samples. Note that, at this point, the temperature decreasing curve indicates the amount of heat being transferred to the environment.

We measured the AVT values against corresponding concentrations for all samples, as indicated in Figure 2. All AVT and concentration data are summarized in Tables 1-4. Since the photothermal effect is an extensive property, it has a concentration dependence, as shown in Figure 2a-d. For the highest chlorophyll concentration of  $7.77 \times 10^{-5}$  g/cm, with an AVT of 65%,  $\Delta T$  reaches 6.3 °C, while the lowest concentration  $(4.27 \times 10^{-5} \text{ g/cm}^2)$  yields the highest AVT of 85% and smallest  $\Delta T$  of 3.8 °C, as expected (Figure 2a). Similar behaviors can be observed in Figure 2b-d. In Figure 2e-h, we plot  $\Delta T$  vs AVT (which scales with concentration) as an important factor for certain energy applications that require transparency of the coatings. As shown in these figures, there are linear relationships between  $\Delta T_{\text{max}}$  and AVT for all thin film samples, indicating that the photothermal effects of these samples are highly correlated to the optical absorption and transmittance.

## 4. DISCUSSION

**4.1. Production of Thermal Energy and Specific Photothermal Coefficient.** The  $\Delta T$  vs time curves shown in Figure 2 provide an experimental basis not only for determining the maximum temperature reachable via photon-activation but also for the photon-to-thermal energy conversion efficiency that is specific to a material (analogous to specific heat). Hence, we develop a new parameter, the specific photothermal coefficient (SPC),  $\mu$ , defined as  $\mu = \dot{Q}/m$ , where  $\dot{Q}$  is the amount of heat produced by the photothermal effect in units of J/s and m is the mass of the material in grams. Therefore,  $\mu$  is in units of J/(g·s). Note that the data used for the calculation of  $\mu$  are based on the thin film samples.

In consideration of the  $\Delta T$  vs time curves shown in Figure 2, the Newtonian cooling law was invoked as

$$V\rho C_p \frac{dT}{dt} = \dot{Q} - UA(T - T_0) \tag{1}$$

where  $\mu$  is the sample temperature in  ${}^{\circ}C$  and  $T_0$  is the initial and ambient temperature, assumed constant during the experiment.  $T-T_0$  represents each  $\Delta T$  value from the  $\Delta T$  vs time curves shown in Figure 2, V is the volume of the sample  $(cm^3)$ ,  $\rho$  is the sample density  $(g/cm^3)$ ,  $C_p$  is the sample specific heat capacity  $(J/(g\cdot K))$ , t is the heating time (s), U is the heat transfer coefficient  $(W/(m^2\cdot K))$  of the sample, A is the sample surface area  $(cm^2)$ , and  $\dot{Q}$  is the heat produced by the photothermal effect in unit of (J/s).

In eq 1, U is the overall heat transfer coefficient that includes the effects of cooling through free convection and radiation. In all test conditions  $\Delta T \ll T_0$ , so the linearized form of the radiation heat transfer equation can be used. The linearized heat transfer coefficient is considered to be

$$h_{\rm r} = 4T_0^3 \varepsilon \sigma$$

Here,  $\varepsilon$  is the surface emissivity and  $\sigma$  is the Boltzmann constant. For  $\Delta T \ll T_0$ ,  $h_{\rm r}$  is constant. The heat loss due to radiation is then given by  $h_{\rm r}A(T-T_0)$ .

The heat loss from the sample to the environment through convection cooling is what  $hA(T - T_0)$  represents. The overall heat transfer coefficient including convection and radiation is

$$U = (h_{\rm r} + h)$$

Figure 3 shows a schematic diagram of the temperature difference  $\Delta T$  vs time curve for analysis. As can be seen in this figure, when the sample is initially and rapidly heated in stage 1,  $\dot{Q} > UA(T-T_0)$ , indicating that heating is greater than the heat loss. In stage 2, the sample temperature reaches a steady state as the heat loss to the environment is equal to the heat gain via the photothermal effect. Therefore, we have  $V\rho C_P \frac{dT}{dt} = \dot{Q} - UA(T-T_0) = 0$  and  $\dot{Q} = UA(T-T_0)$ . In stage 3, since the light source is turned off,  $\dot{Q} = 0$ .

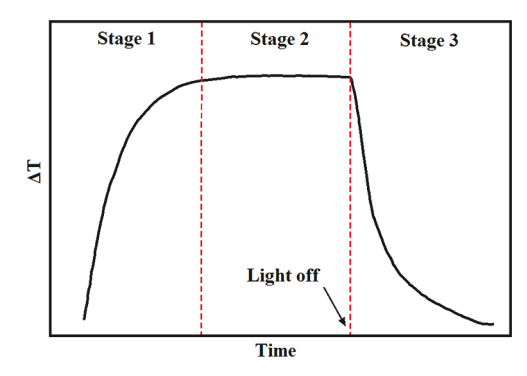


Figure 3. Schematic diagram showing the temperature vs time curve.

The differential equation of eq 1 can be separated into the left-hand side, solely dependent on T, and right-hand side, solely dependent on t; therefore

$$\frac{\mathrm{d}T_{\mathrm{i}}}{\mathrm{d}t} = \frac{\dot{Q}}{V\rho C_{p}} - \frac{UA}{V\rho C_{p}} (T - T_{0})$$

$$= -\frac{UA}{V\rho C_{p}} \left[ (T - T_{0}) - \frac{\dot{Q}}{UA} \right]$$
(2)

$$\frac{1}{(T-T_0) - \frac{Q}{UA}} dT = -\frac{UA}{V\rho C_p} dt$$
(3)

Integrating the differential equation

$$\int \frac{1}{(T - T_0) - \frac{\dot{Q}}{UA}} dT = -\int \frac{UA}{V\rho C_P} dt$$
(4)

yields

$$\ln\left|(T - T_0) - \frac{\dot{Q}}{UA}\right| = -\frac{UA}{V\rho C_p} t + C \tag{5}$$

where *C* is constant. We then have

$$(T - T_0) - \frac{\dot{Q}}{UA} = e^{-(UA/V\rho C_p)t} \cdot e^c = Ce^{-(UA/V\rho C_p)t}$$
(6)

or

$$T - T_0 = Ce^{-(U/V\rho C_p)t} + \frac{\dot{Q}}{UA}$$
(7)

Since  $\dot{Q} = 0$  in stage 3, the expression can be written as

$$T - T_0 = Ce^{-(UA/V\rho C_p)t}$$
(8)

The following expression can be obtained by rewriting eq 8 and taking  $T-T_0=\Delta T$ :

$$\Delta T = C e^{-(UA/V\rho C_p)t} \tag{9}$$

Using eq 9, we can fit the cooling curve in stage 3. Figure 4 shows the typical stage 3 cooling curves that are well-fitted with eq 9 for all samples with AVT = 75%. As shown in this figure, all cooling curves agree well with the exponential decreasing function of eq 9, consistent with the Newtonian cooling behavior.

By fitting the exponential function, we may write the exponential function in the form

$$\Delta T = C_1 e^{C_2 t} \tag{10}$$

where  $C_1$  is constant and  $C_2 = -\frac{UA}{V\rho C_P}$ .

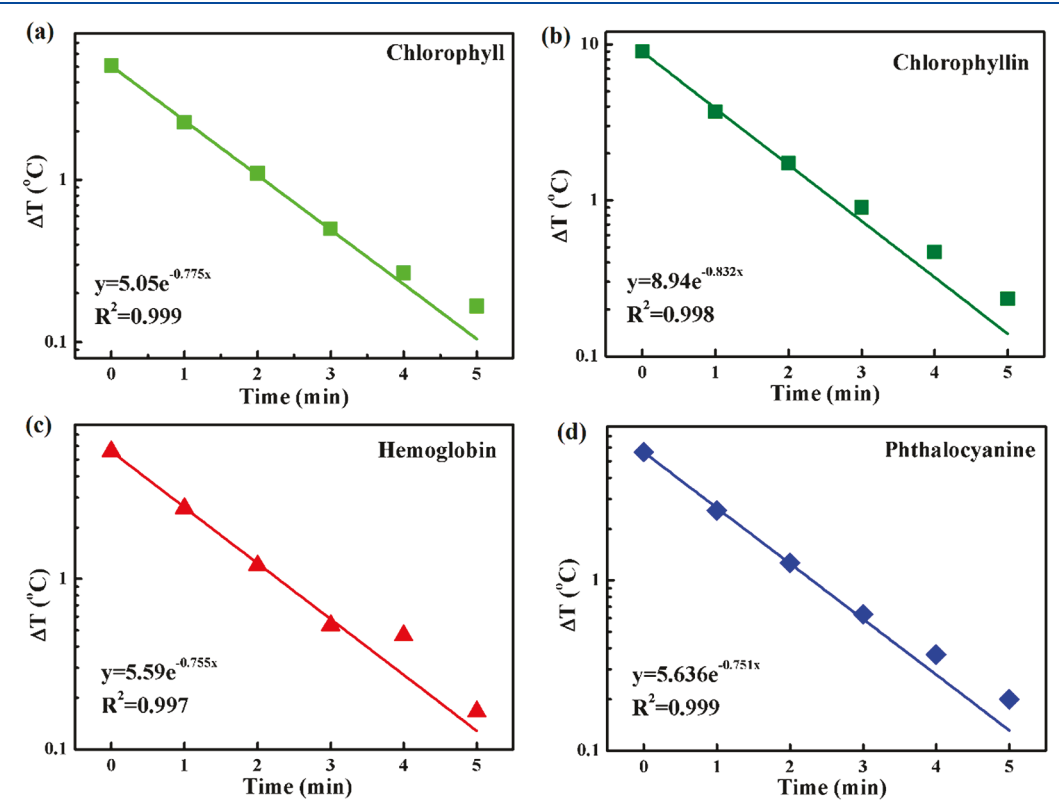


**Figure 4.** Stage 3 cooling curves of the film samples of 75% AVT, fitted with the exponential function of eq 9: (a) chlorophyll, (b) chlorophyllin, (c) hemoglobin, and (d) phthalocyanine (All *y*-axis in logarithmic scale).

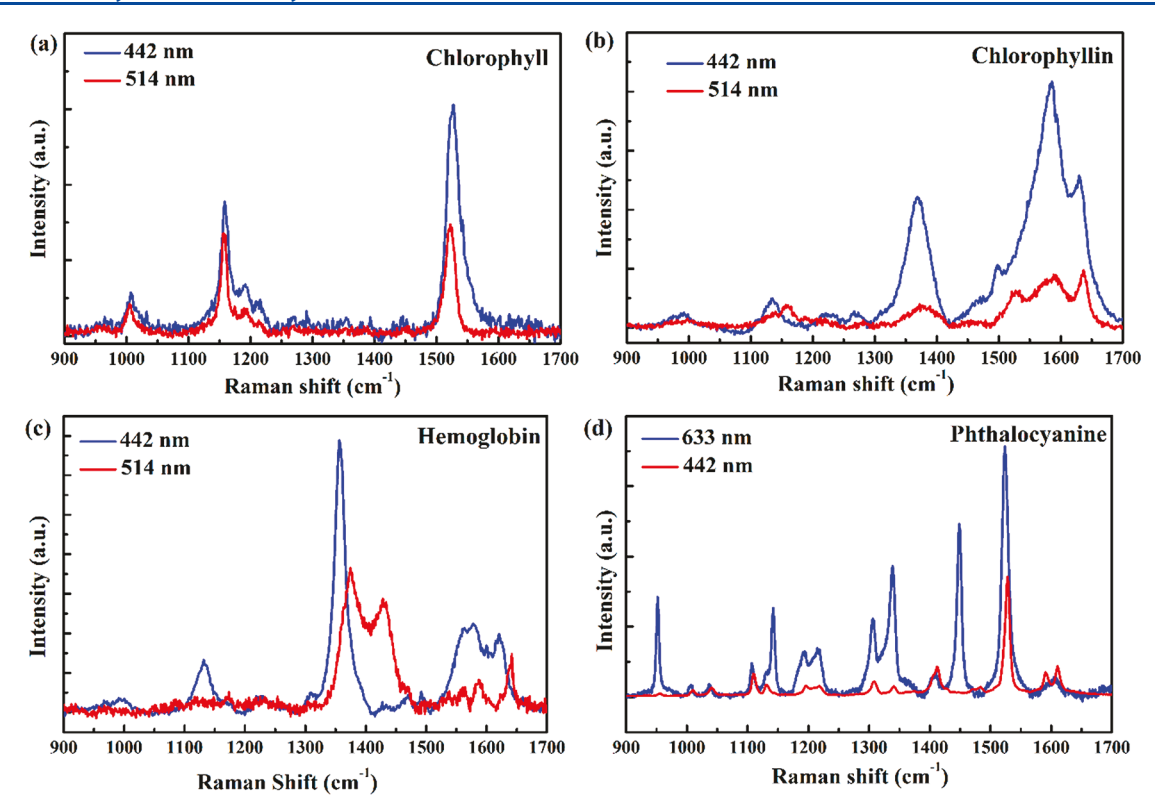


Figure 5. Raman spectra of (a) Chl, (b) Chlin, (c) HB, and (d) Phth on aluminum foils by 442, 514, and 633 nm lasers, respectively.

The  $C_1$  and  $C_2$  values can be obtained from fitting the exponential curve, and U can be calculated through  $C_2$ . Hence,  $\dot{Q}$  can be determined by eq 1.

On the basis of above formulations, the photothermal efficiency,  $\eta$ , can be calculated by the following equation:

$$\eta = \frac{\dot{Q}}{\dot{Q}_{\rm in}} \tag{11}$$

where  $\dot{Q}_{\rm in}$  is the input energy from light source in units of J/s. The maximum temperature difference  $\Delta T_{\rm max}$  denotes the maximum steady state temperature difference from the  $\Delta T$  vs time curve. The dimensions of the sample are  $2.54 \times 2.54 \times 0.11$  cm.  $V \times \rho =$  mass; in addition, the time unit needs to be changed from minutes to seconds, so  $C_2$  in eq 10 can be written as

$$C_2 = -\frac{UA}{60 \times mC_p}$$

The specific heat capacity of the sample can be calculated by the following equation:

$$mC_P = m_{\text{glass}}C_{P,\text{glass}} + m_{\text{polymer}}C_{P,\text{polymer}}$$
  
  $+ m_{\text{materials}}C_{P,\text{materials}}$ 

where  $m_{\rm glass}$  is the mass of the substrate (glass),  $m_{\rm polymer}$  is the mass of the thin film, and  $m_{\rm materials}$  is the mass of the composite materials.  $C_{P,{\rm glass}}$  is the specific heat of the substrate (glass),  $C_{P,{\rm polymer}}$  is the specific heat of the film, and  $C_{P,{\rm materials}}$  is the specific heat of the photothermal materials. Note that the photothermal film is very thin, having a mass only about 0.2-1 mg, which is less than 0.1% of the glass mass. Therefore, the fractions of the polymer and photothermal materials can be ignored for calculating  $mC_P$ :

$$mC_P \approx m_{\rm glass} C_{P,\rm glass} = 1.75 \text{ g} \times 0.84 \text{ J/(g·K)}$$

As mentioned above, by fitting the cooling data in stage 3 with eq 9 in the form of  $y = C_1 e^{C_2 x}$ , U can be calculated using the values from Figures 2 and 4 (see Tables 1–4). Taking chlorophyllin (1.85 × 10<sup>-5</sup> g/cm<sup>2</sup>) as an example (Figure 4b),

$$C_2 = -\frac{UA}{60 \times mC_p} = -0.01387$$

where  $U = 14.539 \text{ W/(m}^2 \cdot \text{K})$ .

By substituting *U* into the equation  $\dot{Q} = UA(T - T_0)$  for stage 2 (isothermal), we obtain the  $\dot{Q}$  value of 0.183 W.

The input photon energy can be determined by incident light power density:

$$\dot{Q}_{in} = 0.1 \text{ (W/cm}^2) \times 2.54^2 \text{ cm}^2 = 0.64516 \text{ W}$$

Therefore, the photothermal efficiency can be calculated by eq

$$\eta = \frac{\dot{Q}}{\dot{Q}_{\rm in}} = \frac{0.183}{0.64516} \times 100\%$$

On the basis of the above equation, the photothermal efficiency of the film on glass containing 1.85  $\times$   $10^{-5}$  g/cm² of chlorophyllin under white light irradiation is 28.4%. In the same way, we have calculated the photothermal efficiencies of other materials in various concentrations, which are summarized in Tables 1–4. The other parameters such as  $\Delta T_{\rm max}$  U,  $\dot{Q}$ , and photothermal efficiency values of Chl, Chlin, HB, and Phth films are also included in Tables 1–4. These data were obtained on the basis of the photothermal experimental data of Figure 2 and calculations using eqs 1–11.

For energy conversion studies, it is important to characterize a system with a material-specific parameter, regardless of its concentration. In this way, the materials can be well-characterized with the unique abilities of photon-to-heat conversion. We define a new material-specific parameter that can quantify the thermal energy produced/converted: specific photothermal coefficient  $\mu$  (SPC), which is similar to what has been achieved for magnetic nanoparticles with the specific absorption rate (SAR). <sup>28</sup> SPC can be expressed by the following:

specific photothermal coefficient  $\mu$ 

$$= \frac{\dot{Q}}{\text{mass of photothermal material}}$$

Using this definition, the specific photothermal coefficients are determined to be  $619 \, J/(g \cdot s)$  for the Chlin film,  $352 \, J/(g \cdot s)$  for the Phth film,  $180 \, J/(g \cdot s)$  for the HB film, and  $129 \, J/(g \cdot s)$  for the Chl film, respectively. Note that the specific photothermal coefficients of these compounds were determined using several concentrations (therefore AVTs), and the data points for a specific compound fall into a small range of error pars; therefore an average value of SPC was used, as shown above. Comparing the SPC values of all four compounds, chlorophyllin has the highest average value of  $619 \, J/(g \cdot s)$ , indicating a greater ability of photon-to-heat conversion. This is consistent with its stronger absorptions near UV and NIR compared to those of other porphyrinic compounds (Figure 1).

4.2. Photothermal Effect of the Porphyrinic Compounds. One of the major issues in the photothermal studies deals with the photon-to-thermal energy conversion associated with the different material classes and electronic structures. As mentioned above, while the metallic materials have been extensively studied in terms of LSPR, the photothermal mechanism of the porphyrinic compounds will require further investigations. Metallic and porphyrinic compounds are sharply juxtaposed with the charge carrier densities. Therefore, the LSPR model is unlikely a photothermal mechanism for the latter due to their very limited charge carrier densities. However, the porphyrinic molecular oscillations are possible contributing factors to conversions of heat via photon irradiation. The photonically activated thermal energy in several porphyrinic compounds are evident in Figure 2 and well-correlated to their absorption spectra in terms of the conversion efficiencies. Further evidence of molecular oscillation-induced photothermal effects was found in the Raman scattering experiments, as shown in Figure 5.

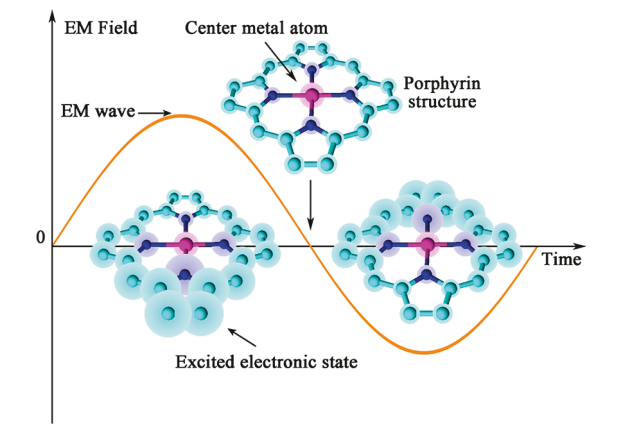
Figure 5 shows the Raman spectra of the chlorophyll (Chl), chlorophyllin (Chlin), hemoglobin (HB), and phthalocyanine (Phth) samples. Each sample was obtained by drop-casting the solution on aluminum foil. Three lasers with 442, 514, and 633 nm wavelengths, respectively, were used for the excitations. In Raman scattering, the incident laser light interacts with the molecular structures, activating vibrations of porphyrins that are associated with phonons and electrons of the system, resulting in an energy shift of the scattered photons. As shown in Figure 5a for the chlorophyll sample, the Raman peaks excited by the 442 and 514 nm laser are both intensified significantly at 1160 and 1540 cm<sup>-1</sup>, respectively. Raman peaks are typically identified as molecular vibrations involving the bonds of the porphyrins, corresponding to the photon absorptions. Raman scattering can be significantly enhanced if the incident photon energy is on the same order of magnitude as the optical absorptions, which are directly associated with the molecular vibration modes of the compounds. This is consistent with the two absorption peaks of chlorophyll at 415 and 664 nm, as shown in Figure 1. However,

since the 514 nm laser is somewhat far from the 664 nm absorption of chlorophyll, the 422 nm laser excitation is more efficient, resulting in a higher peak intensity at 1540 cm<sup>-1</sup>, while that by the 514 nm later appears considerably weaker.

A similar behavior can be seen in Figure 5b for chlorophyllin. For the same reason, the 422 nm laser excitation is responsible for the much more intensified Raman peaks at 1370 and 1580 cm<sup>-1</sup>. According to the absorption spectrum shown in Figure 1, chlorophyllin exhibits a stronger absorption at 400 nm, quite close to the 442 nm laser, therefore giving much higher Raman peak intensities than those by the 514 nm laser. It should be noted that, due to these stronger absorptions near UV and NIR, chlorophyllin is characterized with the highest specific photothermal coefficient. Therefore, the Raman data provide an importance base that the photothermal effect is associated with the molecular vibrations of the porphyrins.

Further evidence can be seen from Figure 5c,d for the HB and Phth samples. Again, the hemoglobin film also exhibits a strong absorption near 400 nm, leading to all 442 nm laser excited peaks being much more intensive compared to those by the 514 nm laser. The situation is quite different for the phthalocyanine sample, as this compound has a stronger and wider absorption beyond 600 nm (Figure 1). This is the reason we chose a 633 nm laser as the excitation. As expected, all Raman peaks of the phthalocyanine sample by the 633 nm laser are more intensified than those by the 442 nm laser, especially the one at 1530 cm<sup>-1</sup> (Figure 5c). The Raman data from Figure 5 show close correlations between the excitations and the absorptions that provide a fundamental physical base for the molecular oscillation-induced photothermal effects of the porphyrins. Note that the molecular vibration should be caused by the decay of the excited state of electrons. This is because the photothermal effect of porphyrinic compounds is based on the photoexcitation process. An earlier study on chlorophyll also reported that the lowest band gap of chlorophyll (extracted from spinach) is 1.83 eV (677 nm),<sup>29</sup> which perfectly matches an absorption peak of chlorophyll shown in Figure 1.

The mechanism of the molecular oscillation-induced photothermal effect (MOIPE) is schematically illustrated in Figure 6. Upon light irradiation, if the incident photon frequency, v (i.e., energy E = hv), is moderately greater than resonance frequency, v<sub>o</sub>, of the electrons associated with the porphyrins, the oscillation is in phase with the incident photon frequency. The magnitude of electron oscillation varies in phase with the



 $\label{eq:Figure 6.} \textbf{ Schematic diagram showing the molecular oscillation-induced photothermal effect (MOIPE) of porphyrin.}$ 

incoming EM wave, as depicted in Figure 6. If the incident photon frequency approaches the resonance frequency,  $v \sim v_{\rm o}$ , then the system is said to be at resonance with the highest charge displacement. In a reasonable frequency range between v and  $v_{\rm o}$ , the incident photons are able to induce significant electron excitations and associated porphyrin molecular vibrations, as evident from the Raman data shown in Figure 6, which provide close correlations between the incident photon energy and the absorptions of the porphyrins.

Therefore, within the range of absorption frequency, the photon-excited electrons establish a distribution of charge displacement and the associated molecular vibrations of porphyrin. With the constant irradiation by the incident light, the local electrons form a collective oscillation of in a perpetual fashion that dissipates in the form of heat, as evidenced in the  $\Delta T$  vs time curves (Figure 2). This molecular-vibration-induced energy dissipation provides the fundamental base for further investigation on the photothermal mechanism of the porphyrin compounds.

## 5. CONCLUSIONS

In this study, we have investigated the photothermal effects of several porphyrinic compounds and determined their specific photothermal coefficients. On the basis of the heating curve data (Figure 2), we conclude that, predictably, all porphyrinic compounds can be photonically activated to exhibit the photothermal effects. This conclusion is drawn on the basis of their unique structural and photon absorption characteristics, as shown in Figure 1. However, due to their different absorption spectra, the specific photothermal coefficient varies among the porphyrinic compounds investigated in this study, with chlorophyllin having the highest SPC value, associated with its stronger absorptions near UV and NIR.

In contrast to the localized surface plasmon resonance (LSPR) observed from metallic conductors, a fundamentally different photothermal mechanism is proposed for the compounds typically with the porphyrins. Raman data show the scattering peaks most intensified by excitations (incident laser light) near the optical absorptions, providing strong evidence for photon-activated molecular vibrations. These vibrations at the particular frequencies correspond closely to the absorptions of porphyrins and directly contribute to photonto-heat conversion. We therefore attribute the photon-activated "molecular resonance" to the photothermal effect in the porphyrinic compounds. However, physically plausible models need to be established for the porphyrinic compounds that are analytical and based on computer simulations. We have also developed a new parameter that can precisely characterize the photothermal effect of a material: the specific photothermal coefficient (SPC). With the  $\Delta T$  vs time data, key parameters related to the photothermal effect are calculated on the basis of the Newtonian cooling law for the porphyrinic compounds investigated in this research.

#### AUTHOR INFORMATION

#### **Corresponding Author**

\*Phone: 513-556-3100. E-mail: shid@email.uc.edu.

ORCID

Yuan Zhao: 0000-0002-8705-6175

#### **Author Contributions**

The manuscript was written through contributions of all authors. All authors have given approval to the final version of the manuscript.

#### **Notes**

The authors declare no competing financial interest.

#### ACKNOWLEDGMENTS

We acknowledge the financial support from the National Science Foundation Grants CMMI-1635089 and EEC-1343568. We thank Dr. Andrew J. Steckl for the use of the Perkin-Elmer spectrophotometer. Dr. Mathias Bonmarin was visiting the University of Cincinnati as Fulbright scholar when the work performed in this paper was initiated.

## REFERENCES

- (1) Cook, L. P.; Brewer, G.; Wong-Ng, W. Structural Aspects of Porphyrins for Functional Materials Applications. *Crystals* **2017**, *7*, 223.
- (2) Saltsman, I.; Goldberg, I.; Balasz, Y.; Gross, Z. Porphine and Pyrrole-substituted Porphyrin from Cyclocondensation of Tripyrrane with Mono-substituted Pyrroles. *Tetrahedron Lett.* **2007**, 48, 239–244.
- (3) Kaduk, J. A.; Wong-Ng, W.; Cook, L. P. Synchrotron X-ray Investigation of  $\alpha$ -chlorohemin,  $C_{34}H_{32}ClFeN_4O_4$ , an Fe-porphyrin. *Solid State Sci.* **2016**, 53, 63–70.
- (4) Crossley, M. J.; Burn, P. L. An Approach to Porphyrin-based Molecular Wires: Synthesis of a Bis (Porphyrin) Tetraone and Its Conversion to a Linearly Conjugated Tetrakisporphyrin System. *J. Chem. Soc., Chem. Commun.* **1991**, *21*, 1569–1571.
- (5) Perlovich, G. L.; Golubchikov, O. A.; Klueva, M. E. Thermodynamics of Porphyrin Sublimation. *J. Porphyrins Phthalocyanines* **2000**, *04*, 699–706.
- (6) Jurow, M.; Schuckman, A. E.; Batteas, J. D.; Drain, C. M. Porphyrins as Molecular Electronic Components of Functional Devices. *Coord. Chem. Rev.* **2010**, 254, 2297–2310.
- (7) Auwärter, W.; Écija, D.; Klappenberger, F.; Barth, J. V. Porphyrins at Interfaces. *Nat. Chem.* **2015**, *7*, 105–120.
- (8) Livshits, V. A.; Blyumenfel'd, L. A. Semiconductor Properties of Porphyrins. *J. Struct. Chem.* **1968**, *8*, 383–388.
- (9) Kobayashi, N.; Nevin, W. A.; Mizunuma, S.; Awaji, H.; Yamaguchi, M. Ring-expanded Porphyrins as an Approach Towards Highly Conductive Molecular Semiconductors. *Chem. Phys. Lett.* **1993**, 205, 51–54.
- (10) Jones, R.; Tredgold, R. H.; Hoorfar, A.; Hodge, P. Electrical Conductivity in Langmuir-blodgett Films of Porphyrins: In-plane and Through-the-film Studies. *Thin Solid Films* **1984**, *113*, 115–128.
- (11) Suslick, K. S.; Chen, C. T. Polymeric Metalloporphyrins for Field Responsive Materials. *Polym. Mater. Sci. Eng.*, Proceedings of the ACS Division of Polymeric Materials Science and Engineering, Washington, DC, USA, Aug 26–31, 1990.
- (12) Chen, C. T.; Suslick, K. S. One-Dimensional Coordination Polymers: Applications to Material Science. *Coord. Chem. Rev.* **1993**, 128, 293–322.
- (13) Zhao, Y.; Sadat, M. E.; Dunn, A.; Xu, H.; Chen, C. H.; Nakasuga, W.; Ewing, R. C.; Shi, D. Photothermal Effect on  $Fe_3O_4$  Nanoparticles Irradiated by White-light for Energy-efficient Window Applications. Sol. Energy Mater. Sol. Cells **2017**, 161, 247–254.
- (14) Zhao, Y.; Dunn, A. W.; Shi, D. Effective Reduction of Building Heat Loss Without Insulation Materials via the Photothermal Effect of a Chlorophyll Thin Film Coated "Green Window". *MRS Commun.* **2019**, 9, 675–681.
- (15) Li, L. L.; Yang, C. J.; Chen, W. H.; Lin, K. J. Towards the Development of Electrical Conduction and Lithium-Ion Transport in a Tetragonal Porphyrin Wire. *Angew. Chem., Int. Ed.* **2003**, 42, 1505–1508.
- (16) Chen, Y. C.; Lee, M. W.; Li, L. L.; Lin, K. J. Electrical and Optical Properties of Porphyrin Single Crystals. *J. Macromol. Sci., Part B: Phys.* **2008**, 47, 955–966.

- (17) Schramm, C. J.; Stojakovic, D. R.; Hoffman, B. M.; Marks, T. J. New Low-Dimensional Molecular Metals: Single-crystal Electrical Conductivity of Nickel Phthalocyanine Iodide. *Science* **1978**, 200, 47–48.
- (18) Zou, Q.; Abbas, M.; Zhao, L.; Li, S.; Shen, G.; Yan, X. Biological Photothermal Nanodots Based on Self-assembly of Peptide—porphyrin Conjugates for Antitumor Therapy. *J. Am. Chem. Soc.* **2017**, *139*, 1921—1927.
- (19) Kwak, B. S.; Kim, B. S.; Song, S. H.; Kim, H. O.; Cho, H. H.; Jung, H. I. Direct Measurement of the in Vitro Hemoglobin Content of Erythrocytes Using the Photo-thermal Effect of the Heme Group. *Analyst* **2010**, *135*, 2365–2371.
- (20) Lu, S.; Min, W.; Chong, S.; Holtom, G. R.; Xie, X. S. Label-free Imaging of Heme Proteins with Two-photon Excited Photothermal Lens Microscopy. *Appl. Phys. Lett.* **2010**, *96*, 113701.
- (21) Huang, X.; Jain, P. K.; El-Sayed, I. H.; El-Sayed, M. A. Plasmonic Photothermal Therapy (PPTT) Using Gold Nanoparticles. *Lasers Med. Sci.* **2008**, 23, 217–228.
- (22) Liu, X.; Shan, G.; Yu, J.; Yang, W.; Ren, Z.; Wang, X.; Xie, X.; Chen, H. J.; Chen, X. Laser Heating of Metallic Nanoparticles for Photothermal Ablation Applications. *AIP Adv.* **2017**, *7*, 025308.
- (23) Niu, J.; Jun Shin, Y.; Lee, Y.; Ahn, J. H.; Yang, H. Graphene Induced Tunability of the Surface Plasmon Resonance. *Appl. Phys. Lett.* **2012**, *100*, 061116.
- (24) Huang, X.; El-Sayed, M. A. Plasmonic Photo-Thermal Therapy (PPTT). *Alexandria Med J* **2011**, 47, 1–9.
- (25) Chen, X.; Chen, Y.; Yan, M.; Qiu, M. Nanosecond Photothermal Effects in Plasmonic Nanostructures. ACS Nano 2012, 6, 2550–2557.
- (26) Chu, M.; Shao, Y.; Peng, J.; Dai, X.; Li, H.; Wu, Q.; Shi, D. Near-infrared Laser Light Mediated Cancer Therapy by Photothermal Effect of Fe<sub>3</sub>O<sub>4</sub> Magnetic Nanoparticles. *Biomaterials* **2013**, *34*, 4078–4088.
- (27) Gao, K.; Li, L.; Lai, T.; Xiao, L.; Huang, Y.; Huang, F.; Peng, J.; Cao, Y.; Liu, F.; Russell, T. P.; Janssen, R. A. Deep Absorbing Porphyrin Small Molecule for High-Performance Organic Solar Cells with Very Low Energy Losses. *J. Am. Chem. Soc.* **2015**, *137*, 7282–7285.
- (28) Monnier, C. A.; Crippa, F.; Geers, C.; Knapp, E.; Rothen-Rutishauser, B.; Bonmarin, M.; Lattuada, M.; Petri-Fink, A. Lock-in Thermography as an Analytical Tool for Magnetic Nanoparticles: Measuring Heating Power and Magnetic Fields. J. Phys. Chem. C 2017, 121, 27164–27175.
- (29) Syafinar, R.; Gomesh, N.; Irwanto, M.; Fareq, M.; Irwan, Y. M. Chlorophyll Pigments as Nature Based Dye for Dye-Sensitized Solar Cell (DSSC). *Energy Procedia* **2015**, *79*, 896–902.
- (30) Zhang, J. Z. Biomedical Applications of Shape-Controlled Plasmonic Nanostructures: A Case Study of Hollow Gold Nanospheres for Photothermal Ablation Therapy of Cancer. *J. Phys. Chem. Lett.* **2010**, *1*, 686–695.